Energy profile of nanobody–GFP complex under force

2015 Phys. Biol. 12 056009

(http://iopscience.iop.org/1478-3975/12/5/056009)

Physical Biology

PAPER

Energy profile of nanobody–GFP complex under force

Kamila Klamecka[1,2], **Philip M Severin**[1], **Lukas F Milles**[1], **Hermann E Gaub**[1] **and Heinrich Leonhardt**[2]

[1] Lehrstuhl für Angewandte Physik and Center for Nanoscience (CeNS), Ludwig-Maximilians-Universität, Amalienstrasse 54, D-80799 Munich, Germany

[2] Department of Biology II and Center for Nanoscience (CeNS), Ludwig-Maximilians-Universität, Großhadernerstr. 2, D-82152 Planegg-Martinsried, Germany

E-mail: gaub@lmu.de

Keywords: single-molecule force spectroscopy, GFP, nanobody, AFM

Supplementary material for this article is available online

OPEN ACCESS

RECEIVED
28 May 2015

REVISED
26 July 2015

ACCEPTED FOR PUBLICATION
6 August 2015

PUBLISHED
10 September 2015

Abstract

Nanobodies (Nbs)—the smallest known fully functional and naturally occuring antigen-binding fragments—have attracted a lot of attention throughout the last two decades. Exploring their potential beyond the current use requires more detailed characterization of their binding forces as those cannot be directly derived from the binding affinities. Here we used atomic force microscope to measure rupture force of the Nb–green fluorescent protein (GFP) complex in various pulling geometries and derived the energy profile characterizing the interaction along the direction of the pulling force. We found that—despite identical epitopes—the Nb binds stronger (41–56 pN) to enhanced GFP than to wild-type GFP (28–45 pN). Measured forces make the Nb–GFP pair a potent reference for investigating molecular forces in living systems both *in* and *ex vivo*.

Introduction

The discovery of heavy-chain-only antibodies (HCAbs) in camelids [1] inspired completely new approaches in antibody engineering. Devoid of light chains, HCAbs recognize their antigens using single protein domains—unlike their conventional counterparts, which need parts of both heavy and light chain to bind the epitope. Derived from HCAbs, so-called nanobodies (Nbs) constitute the smallest functional antigen-binding domain (for review see [2]). Their average molecular mass of about 15 kDa makes them ten times smaller than typical antibodies. Yet, they remain competitive in their binding affinity and specificity. Nbs can be raised against a desired antigen, easily cloned and expressed in heterologous hosts, including bacteria [3]. Interestingly, they combine the advantages of conventional antibodies with greatly improved tissue permeability owing to their reduced size and increased hydrophilicity [4]. Nbs show a high degree of identity with human type 3 VH domains and humanization strategies have been proposed [5, 6]. Therefore, it is not surprising that Nbs were considered potent agents in therapeutics and immunodiagnostic methods early on.

Nbs are versatile reagents that are useful in a broad variety of applications. Of particular interest is the use of Nbs in *in vivo* imaging techniques [7, 8]. Non-invasive (and repeatable) visualization is for example important when screening the progress of a disease. Here, Nbs' small size and lack of adverse effects help bypass the limitations typical of conventional antibodies. In recent years, Nbs have proven successful in therapy [9, 10] and their bispecific derivatives are expected to aid in tumor treatment by crosslinking otherwise unrelated antigens [11, 12]. Medical uses beyond oncology [13, 14] include monitoring arthritis [15], atherosclerosis [16] and other inflammatory diseases [17, 18].

Various green fluorescent protein (GFP)-binders have been identified amongst the broad range of available Nbs [19, 20]. One of them stands out due to its multitude of applications [19, 21]. This GFP-binding Nb, coupled to solid support is widely used for purification of GFP-fusion proteins and the Nb–GFP complex has proven stable under harsh conditions including high salt, temperatures reaching 65 °C or extremes of pH [22].

Widespread use of GFP as a nontoxic, universal fluorescent protein tag throughout cell biology labs motivated the focus of this study. Given the vivid

interest in the Nb technology, its expansion over even broader areas relying on protein–protein interactions can be anticipated. This in turn brings up the need for a detailed biophysical characterization of the Nb binding to its target. We intend to bridge the gap between existing bulk-derived biochemical characteristics of the Nb–GFP system and the requirements of single molecule approaches by characterizing a single complex under force load. This aspect is relevant for both *in vivo* mechanical studies of protein interactions as well as single molecule manipulation techniques such as Single-Molecule Cut&Paste [23, 24]. In another work we described this bond relatively to other molecular interactions [25].

Here, we analyze the binding strength of a model Nb in complex with its antigen by means of single-molecule force spectroscopy utilizing atomic force microscopy (AFM), a well-established technique for mechanical studies of biomolecules. The force range typically resolved by the AFM makes it a method of choice for protein unfolding [26, 27] as well as protein–protein interactions [28–30].

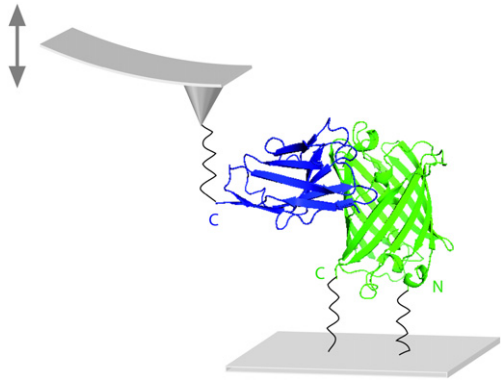

Figure 1. Schematic visualization of the experiment. Covalent anchors are used to immobilize the GFP construct on the glass surface on N-, C- or both termini. In each case polymer spacers are used to anchor the protein at a given distance from surface and cantilever. Depending on the GFP construct, additional protein spacers might be present at either terminus. Within a single measurement cycle, the cantilever functionalized with the nanobody is brought in contact with the GFP-decorated surface and then retracted and a force-extension curve is recorded.

Materials and methods

GFP constructs

Three enhanced GFP (eGFP) and four wild-type GFP (wtGFP) constructs were investigated. Amongst them, all eGFPs and two wtGFPs (one N- and one C-terminally anchored) displayed complete similarity of the epitope amino acid composition to the GFP for which the crystal structure is determined [19]. The other N-terminally anchored wtGFP as well as the double-anchored wtGFP carried a point mutation within the Nb–GFP interface—glutamic acid at position 142 of GFP was substituted by glutamine (see supplementary information for details).

Nanobody

The only two cysteines present in the native Nb form a disulfide bond stabilizing the protein's tertiary structure. Introduced C-terminal cysteine does not perturb the folding of the protein and is readily available for immobilization. Successful GFP binding to surface-immobilized Nb was proven prior to the AFM experiments (data not shown).

All proteins were expressed in *E. coli* and purified using affinity chromatography.

Anchoring chemistry

GFP was site-specifically anchored to the surface in three different attachment geometries, comprising single attachment via N- or C-terminus and double, where the protein was immobilized via both termini, as schematically presented in figure 1.

Generally, the behavior of a complex under external load may be greatly influenced by the positions of the anchors, which restrict the molecules spatially. Variation in anchoring geometries was meant to reveal differences in unbinding pathways—if present—due to a stiffer double connection as compared to a single one. Single anchoring of eGFP was achieved through engineered terminal cysteine binding (through the thiol group of its side chain) to maleimide groups exposed on the PEGylated glass surface, as described in [31]. In short, TCEP-reduced GFP was applied on amino-silanized slides at a concentration of 0.5–1 mg ml^{-1}. After 1 h of incubation at room temperature, unbound protein was washed away with 1x PBS. Maleimide chemistry was also applied to cantilevers using the same steps as for glass slide functionalization. Using Immobilized TCEP Disulfide Reducing Gel (Thermo Scientific) proved to be an efficient method for breaking protein dimers, yet gentle enough to leave the Nb's internal disulfide intact.

Cysteine dimerizes upon oxidation, forming cystine, hence—to avoid oligomeric chains of GFP probed in an unknown orientation—double anchoring required another attachment chemistry. Both double-anchored enhanced and wild-type GFP were therefore attached via hAGT (also known as SNAP-tag) that covalently binds to benzylguanine. The specificity and irreversibility of the hAGT tag reaction with its substrate [32] indicate high probability of successful coupling of the second anchor once the first handle has bound its partner on the surface. Double-anchored GFP constructs contained additional protein spacers of four titin Ig domains at each end. The Ig domains—able to withstand forces of at least 150 pN at loading rates comparable to our experiments—display much higher mechanical stability than GFP so they can be treated as stable linkers [26]. Purified hAGT-tagged proteins [33] were bound to an O_6-benzylguanine-functionalized glass surface as described in

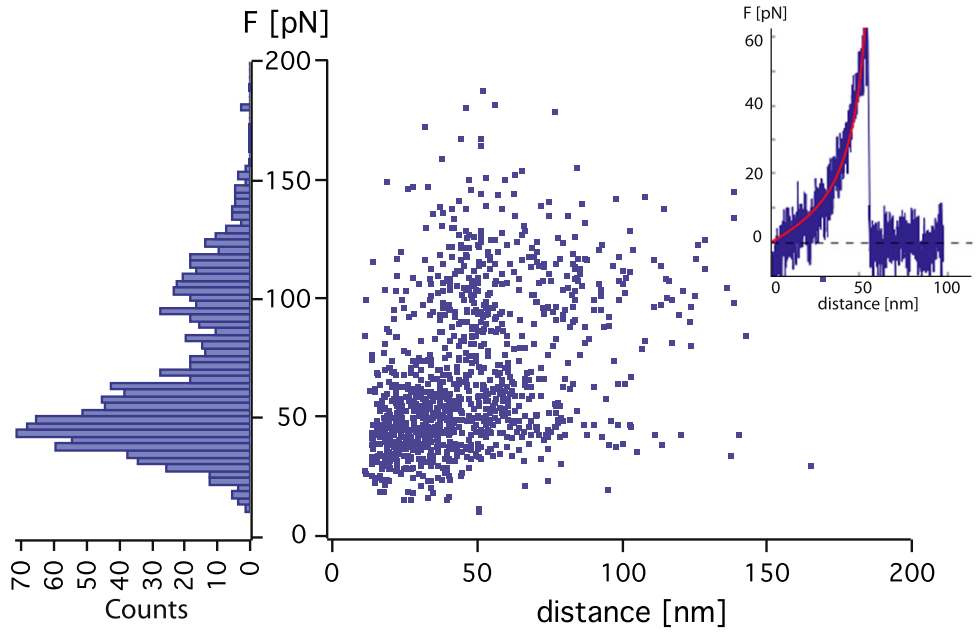

Figure 2. Typical force-extension plot for raw data (here: eGFP N + C anchored). Each point represents the distance and the force at which the Nb–GFP complex was separated. Two distinct populations represent single (∼50 pN) and double (∼100 pN) rupture events. Projection of all points onto the force axis results in a histogram from which the most probable rupture force is obtained. The inset shows an exemplary single-event force–distance curve fitted with WLC (red line).

[32]. Single-anchored wtGFP was immobilized via either an hAGT tag or a short ybbR peptide tag [34] as described earlier in [35]. All these anchoring chemistries are straightforward and efficient and have been successfully used for protein immobilization before [31–33].

Force spectroscopy—data collection

Single molecule force spectroscopy experiments were performed using commercial MFP-3D AFM (Asylum Research) and a custom built instrument with an MFP-3D controller. Two types of cantilevers were used: MLCT (cantilever C) by Bruker and Biolever mini (BL-AC40TS-C2) by Olympus. For each measurement cantilever spring constants were calibrated in solution using the equipartition theorem [36]. The Nb–GFP bond strength was tested in a series of measurements at various pulling speeds ranging from 300 to 10 000 nm s^{-1} and for different attachment geometries of GFP to the surface. A single measurement cycle consisted of approach, short (<1 s) dwell at the surface and retraction of the Nb-functionalized cantilever with constant velocity. An exemplary force-extension plot resulting from a series of measurements for a single GFP construct is shown in figure 2.

Each point is derived from a single force curve (see inset in figure 2) recorded for cantilever retraction. Between single approach-retraction cycles the *x*–*y* piezo stage was moved so that each time a different surface-bound molecule was exposed to the same molecule on the cantilever. Based on the known geometry of protein attachment as well as the chemistry used, curves displaying single rupture events within the expected distance range were selected for further analysis.

Data analysis

Since bond dissociation—also under force—is a thermally driven process, probing the bond several times results in a rupture force distribution. Force-distance curves displaying a single peak were selected for the analysis. The wormlike chain model [37] was used to fit the raw data and extract force and extension values for each single event. For each pulling velocity the most probable rupture force and the respective loading rate were derived from Gaussian fits to force and loading rate histograms obtained for hundreds of recorded events (figure 3).

Loading rate of every single force-distance curve was determined by linear fit to the slope of the measured force at the last 3 nm preceding the rupture. A dynamic force–loading rate spectrum for each construct was plotted in a semi-log plot and fitted using the two-state Bell–Evans model [38, 39].

Results

We have characterized the rupture forces of Nb bound to wtGFP and eGFP and reconstructed the energy profile of these complexes.

The Nb–GFP complex was probed with different pulling velocities ranging from 300 nm s^{-1} to 10 μm s^{-1}. The most probable rupture force (F^*) was obtained by fitting a Gaussian to the distribution of measured rupture forces and then plotted against the

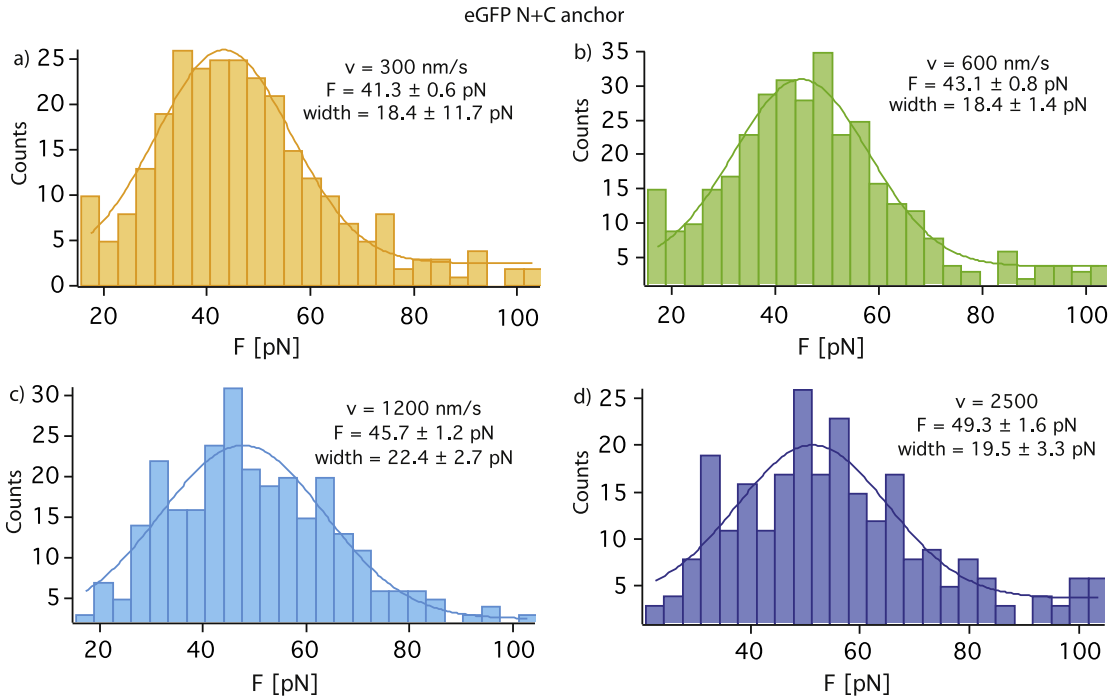

Figure 3. Exemplary results for a series of measurements obtained for one GFP-Nb complex (eGFP, N + C anchor); pulling speeds: (a) 300 nm s^{-1}, (b) 600 nm s^{-1}, (c) 1200 nm s^{-1}, (d) 2500 nm s^{-1}. Gaussian fits to the force histograms yield the most probable rupture forces; here the width parameter is defined as $\sqrt{2}^*$ standard deviation. The most probable rupture force shifts towards higher values with increasing pulling velocities.

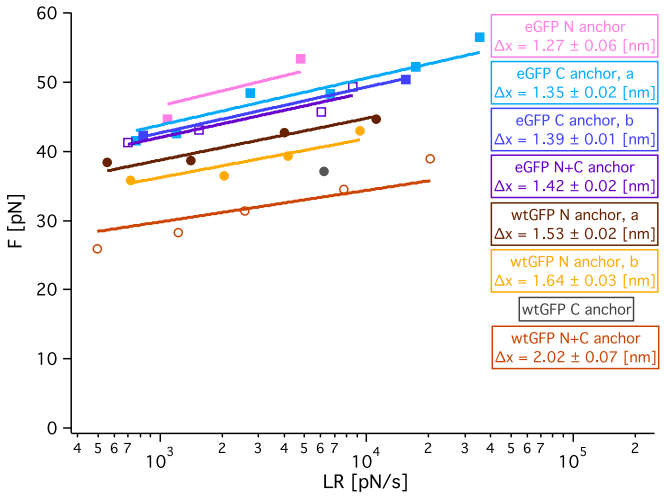

Figure 4. Dynamic force spectrum of Nb–GFP complexes obtained based on pulling velocities ranging from 300 to 10 000 nm s^{-1}. Data points for eGFP are shown with square markers and wtGFP with circle ones; solid markers denote single-anchored GFP (N- or C-terminally) and open ones double-anchored GFP. Data were fitted to the Bell–Evans model using literature off-rate values for wtGFP ($k_{off} = 1.45 \times 10^{-4}\ s^{-1}$) [19] and eGFP ($k_{off} = 1.24 \times 10^{-4}\ s^{-1}$) [40].

respective loading rate ($\dot{F}$). The linear two-state Bell–Evans model (equation (1)) was used to fit the data, with k_{off} describing the dissociation rate at zero force —fixed at the established literature values of $1.45 \times 10^{-4}\ s^{-1}$ for wtGFP [19] and $1.24 \times 10^{-4}\ s^{-1}$ for eGFP [40]

$$F^* = \frac{k_B T}{\Delta x} \ln \frac{\dot{F} \Delta x}{k_B T \cdot k_{off}}. \quad (1)$$

Here Δx denotes the position of the energy barrier, which has to be overcome to dissociate the complex and $k_B T$—the thermal energy of the complex. Literature values of off-rates (k_{off}) were used for fitting since the range of loading rates covered was not broad enough to determine the parameter with reasonable accuracy.

We observed separate characteristic force regimes for wtGFP and eGFP, as shown in figure 4.

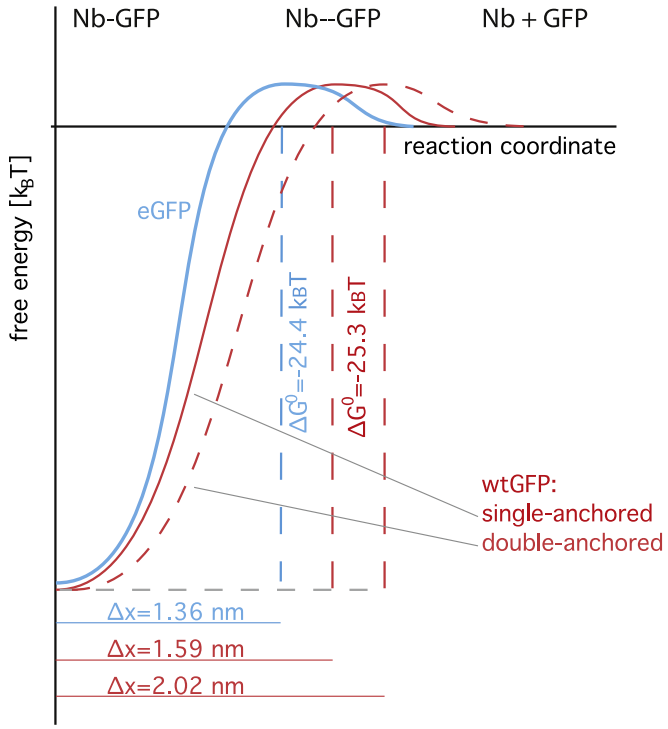

Figure 5. Energy profile of the Nb–GFP complex along the direction imposed by the pulling force. The energy barrier appears 17% shifted—from 1.36 nm (eGFP) to 1.59 nm (single-anchored wtGFP), and even further to 2.02 nm (i.e. by 49%) for double-anchored wtGFP.

The Nb bound to eGFP can withstand forces from 41 to 56 pN, whereas in complex with wtGFP ruptures already at 28–45 pN. For increased clarity, the data are presented in this plot without error bars ('width' in the force histograms). One should note that broad distribution of the measured forces is intrinsic to the technique as it stems from thermal fluctuations of the system (more significant at lower force range), and so does not diminish the significance of its results. Linear dependence of force on logarithm of loading rate suggested a single energy barrier along the reaction coordinate imposed by the direction of the acting force. The obtained energy profiles are graphically presented in figure 5. There is no indication of a significant activation barrier on the dissociation pathway of the Nb–GFP complex—the energy needed to separate the molecules corresponds mainly to the depth of the potential well confining the bound complex.

Interestingly, we observed a 17% broader potential width for single-anchored wtGFP as compared to eGFP, and an even broader one (by 49%) for double-anchored wtGFP (mean values of $\Delta x = 1.36$ nm for eGFP, $\Delta x = 1.59$ nm for single-anchored wtGFP and $\Delta x = 2.02$ nm for double-anchored wtGFP). Using literature values of K_D: 0.59 nM for eGFP–Nb [40] and 1.4 nM for wtGFP-Nb [19], we obtained binding free energies of $-24.4\,k_BT$ for eGFP and $-25.3\,k_BT$ for wtGFP. Following Kramers theory [41, 42], assuming an attempt frequency ν (describing passage of the energy barrier) of the order of 10^7 results in

$$k_{\text{off}} = \nu e^{-\frac{\Delta G^0}{k_B T}} \tag{2}$$

$k_{\text{off}} \sim 10^{-4}$, that is consistent with the known off rates of this complex.

Discussion

In this study we obtained rupture forces for Nb bound to wtGFP and eGFP. For all tested GFP constructs, the Nb-eGFP complex on average withstands higher forces than the Nb-wtGFP one. Moreover, the measured force does not depend markedly on the anchoring geometry. We also found that a point mutation within the Nb-binding site of GFP (E142Q) does not change the rupture characteristic of the complex. This, as well as the separate force regimes observed for the two types of GFP, leads to a conclusion that Nb–GFP binding strength is mainly affected by the chromophore-dependent internal structure more than by the epitope itself, which is in line with the already known ability of the Nb to modulate spectral properties of GFP by binding a protein conformation that is also stabilised by the mutation present in eGFP [19].

Intuitively, one could expect a difference in rupture force between single- and double-anchored GFPs. Single attachment point offers much more flexibility for the protein complex to spatially orientate along the acting force, while fixing the GFP at both termini restricts its freedom of movement the more the complex extends. The stiffer two-point attachment should then result in GFP β-barrel held rather vertically upon

extension and the Nb 'peeling off' or sliding from the side of GFP. Indeed, data for wtGFP point in this direction. In single-anchored GFP pulling by Nb, the whole interaction interface of the complex aligned along the pulling direction ruptures in an all or nothing event. Contact between the two protein surfaces is rapidly lost, hence the smaller potential width (Δx). In case of double-anchored GFP, gradual loss of contact between the Nb and its epitope manifests itself in a higher variance and lowering of the rupture force that yields a broader potential width. This distinction however does not apply to the eGFP constructs, which withstand higher forces when pulled on in complex with Nb—high enough to unfold the N-terminal α-helix, which occurs at around 35 pN and contributes additional 2.9 nm to the effective spacer length [43]. Hence, the complex—although double-anchored—effectively experiences only a single (shorter) anchor and behaves accordingly in response to stretching.

Double anchoring in both cases (wtGFP and eGFP) remains disputable as proteins which successfully attached with only one of the binding domains are virtually indistinguishable from those tethered at both termini. On the other hand, dense surface functionalization and flexibility of the protein linkers between the GFP barrel and the anchors suggest high likelihood of the second domain coupling once the first one is attached. That same flexibility, in turn, allows a lot of freedom in the distance between the two anchors of the same GFP. As a result, the construct may be tilted and skewed when probed and the effect of double anchoring lost.

Due to limited loading rate range covered by the AFM, the x intercept in the Bell–Evans fits was fixed at the literature values of k_{off}, which resulted in negligible error bars for the Δx values calculated from the fits' slopes. This approach holds true for unbinding reaction proceeding along the thermal path, which not necessarily is the case here, yet yielded reasonable values for energy barrier position for an antibody–antigen system. Along this line, the fact that the steepness of the binding potential increases with the acting force explains the anticorrelation of the potential width with respect to rupture force, given that k_{off} is constant. In other words, since the barrier heights (here: binding energies) differ only slightly, reaching the energy maximum with a higher slope of the energy profile occurs over a shorter distance and thus at higher unbinding force.

Nb–GFP interface

GFP has a structure of a β-barrel with both its N- and C-terminus protruding from the same side of its structure. This enables GFP anchoring to the surface via either of its termini as well as via both simultaneously, keeping its overall orientation relative to the surface unchanged. Moreover, upon GFP immobilization, the epitope recognized by the Nb—is exposed, as it is located on the lateral side, close to the opposite end of the β-barrel. Similarly, anchoring the Nb to the cantilever via its C-terminus, should leave its binding site unaffected. Accessibility of the epitope is a prerequisite for efficient single molecule probing of specific interactions, which should not be hindered by unfavorable attachment to the solid support.

Each of the three complementarity-determining regions of the Nb contribute to its binding to GFP, accomplished mostly by electrostatic interactions and a single hydrophobic contact. The epitope extends over 672 Å^2 at the exposed loop region between the strands 6 and 7 of the GFP β-barrel [19].

Site-specific protein attachment provides a controlled and uniform probing geometry, which is crucial for the correct interpretation of the obtained results. In case of protein anchoring utilizing maleimide-thiol chemistry, it is important to ensure that the attachment results solely from the engineered cysteine coupling to surface and that no protein-intrinsic cysteine reacts with maleimide. In its native state, GFP contains two reduced cysteines at positions 48 and 70. Cys70 is buried inside the β-barrel, while Cys48 is partially solvent exposed. However, it is not available for binding to maleimide on the surface (data not shown), demonstrating that coupling of GFP was site-specific as desired.

Specificity of interactions

In force measurements it is crucial to discriminate specific from unspecific interactions to reduce the impact on the analysis by the latter. In protein unfolding studies this is often accomplished by including an extra domain in the construct, which unfolds at lower force than the protein of interest, yielding a fingerprint in the force-extension curves. The relatively low rupture forces measured for the Nb–GFP complex pose a difficulty in finding a compatible protein signature for this purpose. Therefore we analyzed a number of negative control experiments where binding sites on the Nb or GFP were blocked with an excess of the respective binding partner as well as measurements utilizing incompletely functionalized (i.e. lacking the protein) cantilevers or surfaces. In all cases the interaction frequency was drastically reduced as compared to specific Nb–GFP probing (see supplementary information).

Summary

In response to the emergence of protein-based single-molecule manipulation techniques, mechanistic analysis of the Nb–GFP interaction bridges the gap between available bulk-derived affinity data and relevant to single molecule force characteristic describing an isolated complex. The fact that the measured forces are in the range of DNA oligonucleotides unbinding [44] makes the Nb–GFP complex a promising candidate as a reference in protein-based comparative force

assays. This indicates the applicability of the Nb–GFP complex in determining strength of yet uncharacterized protein pairs. Furthermore, one can imagine the application of Nbs as molecular force sensors also *in vivo*.

Acknowledgments

The authors thank Dr Frauke Gräter, Dr Diana Pippig and Dr Jonas Helma for helpful discussions and Daniela Aschenbrenner for critically reading the manuscript. This work was supported by the Deutsche Forschungsgemeinschaft (SFB 1032 to HEG and SPP 1623 to HL). KK and PMS acknowledge financial support by the Elite Network of Bavaria (International Doctorate Program NanoBioTechnology) and Nanosystems Initiative Munich.

References

[1] Hamers-Casterman C *et al* 1993 Naturally occurring antibodies devoid of light chains *Nature* **363** 446–8
[2] Helma J, Cardoso M C, Muyldermans S and Leonhardt H 2015 Nanobodies and recombinant binders in cell biology *J. Cell Biol.* **209** 633–44
[3] Arbabi Ghahroudi M, Desmyter A, Wyns L, Hamers R and Muyldermans S 1997 Selection and identification of single domain antibody fragments from camel heavy-chain antibodies *FEBS Lett.* **414** 521–6
[4] Riechmann L and Muyldermans S 1999 Single domain antibodies: comparison of camel VH and camelised human VH domains *J. Immunol. Methods* **231** 25–38
[5] Vincke C, Loris R, Saerens D, Martinez-Rodriguez S, Muyldermans S and Conrath K 2009 General strategy to humanize a camelid single-domain antibody and identification of a universal humanized nanobody scaffold *J. Biol. Chem.* **284** 3273–84
[6] Vaneycken I *et al* 2010 *In vitro* analysis and *in vivo* tumor targeting of a humanized, grafted nanobody in mice using pinhole SPECT/micro-CT *J. Nucl. Med.: Official Publ., Soc. Nucl. Med.* **51** 1099–106
[7] Chakravarty R, Goel S and Cai W 2014 Nanobody: the 'magic bullet' for molecular imaging? *Theranostics* **4** 386–98
[8] Rothbauer U *et al* 2006 Targeting and tracing antigens in live cells with fluorescent nanobodies *Nat. Methods.* **3** 887–9
[9] Vandenbroucke K *et al* 2010 Orally administered *L. lactis* secreting an anti-TNF nanobody demonstrate efficacy in chronic colitis *Mucosal Immunol.* **3** 49–56
[10] Overbeke W V *et al* 2014 Chaperone nanobodies protect gelsolin against MT1-MMP degradation and alleviate amyloid burden in the gelsolin amyloidosis mouse model *Mol. Ther.: J. Am. Soc. Gene Ther.* **22** 1768–78
[11] Els Conrath K, Lauwereys M, Wyns L and Muyldermans S 2001 Camel single-domain antibodies as modular building units in bispecific and bivalent antibody constructs *J. Biol. Chem.* **276** 7346–50
[12] Hmila I *et al* 2010 A bispecific nanobody to provide full protection against lethal scorpion envenoming *FASEB J.: Official Publ. Fed. Am. Soc. Exp. Biol.* **24** 3479–89
[13] Cortez-Retamozo V *et al* 2004 Efficient cancer therapy with a nanobody-based conjugate *Cancer Res.* **64** 2853–7
[14] Altintas I, Kok R J and Schiffelers R M 2012 Targeting epidermal growth factor receptor in tumors: from conventional monoclonal antibodies via heavy chain-only antibodies to nanobodies *Eur. J. Pharm. Sci.: Official J. Eur. Fed. Pharm. Sci.* **45** 399–407
[15] Zheng F *et al* 2014 Molecular imaging with macrophage CRIg-targeting nanobodies for early and preclinical diagnosis in a mouse model of rheumatoid arthritis *J. Nucl. Med.: Official Publ., Soc. Nucl. Med.* **55** 824–9
[16] Broisat A *et al* 2012 Nanobodies targeting mouse/human VCAM1 for the nuclear imaging of atherosclerotic lesions *Circ. Res.* **110** 927–37
[17] Baral T N *et al* 2006 Experimental therapy of African trypanosomiasis with a nanobody-conjugated human trypanolytic factor *Nat. Med.* **12** 580–4
[18] Stijlemans B *et al* 2011 High affinity nanobodies against the Trypanosome brucei VSG are potent trypanolytic agents that block endocytosis *PLoS Pathog.* **7** e1002072
[19] Kirchhofer A, Helma J, Schmidthals K, Frauer C, Cui S, Karcher A *et al* 2010 Modulation of protein properties in living cells using nanobodies *Nat. Struct. Mol. Biol.* **17** 133–8
[20] Fridy P C *et al* 2014 A robust pipeline for rapid production of versatile nanobody repertoires *Nat. Methods* **11** 1253–60
[21] Herce H D, Deng W, Helma J, Leonhardt H and Cardoso M C 2013 Visualization and targeted disruption of protein interactions in living cells *Nat. Commun* **4** 2660
[22] Rothbauer U, Zolghadr K, Muyldermans S, Schepers A, Cardoso M C and Leonhardt H 2008 A versatile nanotrap for biochemical and functional studies with fluorescent fusion proteins *Mol. Cell. Proteomics: MCP* **7** 282–9
[23] Kufer S K, Puchner E M, Gumpp H, Liedl T and Gaub H E 2008 Single-molecule cut-and-paste surface assembly *Science* **319** 594–6
[24] Strackharn M, Pippig D A, Meyer P, Stahl S W and Gaub H E 2012 Nanoscale arrangement of proteins by single-molecule cut-and-paste *J. Am. Chem. Soc.* **134** 15193–6
[25] Aschenbrenner D, Pippig D A, Klamecka K, Limmer K, Leonhardt H and Gaub H E 2014 Parallel force assay for protein-protein interactions *PloS One* **9** e115049
[26] Rief M, Gautel M, Oesterhelt F, Fernandez J M and Gaub H E 1997 Reversible unfolding of individual titin immunoglobulin domains by AFM *Science* **276** 1109–12
[27] Bull M S, Sullan R M, Li H and Perkins T T 2014 Improved single molecule force spectroscopy using micromachined cantilevers *ACS Nano* **8** 4984–95
[28] Florin E L, Moy V T and Gaub H E 1994 Adhesion forces between individual ligand-receptor pairs *Science* **264** 415–7
[29] Herman P, El-Kirat-Chatel S, Beaussart A, Geoghegan J A, Foster T J and Dufrene Y F 2014 The binding force of the staphylococcal adhesin SdrG is remarkably strong *Mol. Microbiology* **93** 356–68
[30] Eghiaian F, Rico F, Colom A, Casuso I and Scheuring S 2014 High-speed atomic force microscopy: imaging and force spectroscopy *FEBS Lett.* **588** 363–8
[31] Blank K, Morfill J and Gaub H E 2006 Site-specific immobilization of genetically engineered variants of Candida antarctica lipase B *Chembiochem.: Eur. J. Chem. Biol.* **7** 1349–51
[32] Kufer S K *et al* 2005 Covalent immobilization of recombinant fusion proteins with hAGT for single molecule force spectroscopy *Eur. Biophys. J.: EBJ* **35** 72–8
[33] Kindermann M, George N, Johnsson N and Johnsson K 2003 Covalent and selective immobilization of fusion proteins *J. Am. Chem. Soc.* **125** 7810–1
[34] Wong L S, Thirlway J and Micklefield J 2008 Direct site-selective covalent protein immobilization catalyzed by a phosphopantetheinyl transferase *J. Am. Chem. Soc.* **130** 12456–64
[35] Limmer K, Pippig D A, Aschenbrenner D and Gaub H E 2014 A force-based, parallel assay for the quantification of protein–DNA interactions *PloS One* **9** e89626
[36] Butt H J and Jaschke M 1995 Calculation of thermal noise in atomic-force microscopy *Nanotechnology* **6** 1–7
[37] Marko J F and Siggia E D 1995 Statistical mechanics of supercoiled DNA *Phys. Rev.* E **52** 2912–38
[38] Bell G I 1978 Models for the specific adhesion of cells to cells *Science* **200** 618–27
[39] Evans E and Ritchie K 1997 Dynamic strength of molecular adhesion bonds *Biophys. J.* **72** 1541–55
[40] Kubala M H, Kovtun O, Alexandrov K and Collins B M 2010 Structural and thermodynamic analysis of the GFP:GFP–nanobody complex. *Protein Sci.: Publ. Protein Soc.* **19** 2389–401

[41] Kramers H A 1940 Brownian motion in a field of force and the diffusion model of chemical reactions *Physica* **7** 284–304
[42] Evans E and Williams P 2002 Dynamic force spectroscopy *Physics of Bio-Molecules and Cells Physique Des Biomolécules Et Des Cellules.* (*Les Houches—Ecole d'Ete de Physique Theorique* vol 75) ed F Flyvbjerg *et al* (Berlin: Springer) pp 145–204
[43] Dietz H and Rief M 2004 Exploring the energy landscape of GFP by single-molecule mechanical experiments *Proc. Natl Acad. Sci. USA* **101** 16192–7
[44] Schumakovitch I, Grange W, Strunz T, Bertoncini P, Guntherodt H J and Hegner M 2002 Temperature dependence of unbinding forces between complementary DNA strands *Biophys. J.* **82** 517–21